31.0 ACCUMULATIVE ROLL BONDING OF ALUMINUM SHEETS TOWARD LOW TEMPERATURE SUPERPLASTICITY

Brady McBride (Mines)
Faculty: Kester Clarke (Mines)
Industrial Mentors: Paul Wilson (Boeing), John Carpenter (LANL), Eric Payton (AFRL)

This project initiated in Fall 2017. The research performed during this project will serve as the basis for a Ph.D. thesis program for Brady McBride.

31.1 Project Overview and Industrial Relevance

Accumulative roll bonding (ARB) is a severe plastic deformation technique used to produce ultra-fine-grained material by introducing large plastic strains via rolling [31.1]. The surfaces of two sheets are wire-brushed, stacked and roll bonded together in a conventional rolling mill [31.1]. After rolling, the material is sectioned in half and the process is repeated. A single-pass, 50% rolling reduction is commonly employed to ensure adequate bonding and to retain the original dimensions after each cycle [31.1]. The ARB process is largely different from conventional rolling processes in that heavy, unlubricated, single-pass reductions are used. This imparts redundant shear into the surface of the rolled material which is introduced through-thickness with subsequent roll bonding cycles [31.2]. The combination of redundant shear and large rolling reductions ultimately lead to grain refinement.

ARB is attractive in its ability to produce ultrafine-grained material with conventional processing equipment while maintaining consistent sample geometry. With the accumulation of large strains, dislocation cell structures form within the material that further develop into refined grains [31.3]. Ultrafine grains (~250 nm) produced after 5 cycles of ARB in Al 5083 have exhibited tensile elongations in excess of 200% for strain rates of 10^{-3} s^{-1} at 200 °C [31.3]. In comparison, superplastic deformation of Al 5083 produced with conventional processing methods typically requires temperatures of 500 °C and strain rates above 10^{-3} s^{-1} to produce elongations around 300%. Enhanced superplasticity provided by the ARB process would be beneficial to superplastic sheet forming operations where reduced temperatures and/or increased strain rates could lead to cost savings and reduced die wear. Additionally, ARB processing may produce sheets that retain a submicron grain structure after forming operations, leading to increased strength in the final part.

31.2 Previous Work – Characterizing continuous recrystallization during static annealing

Previous work for this project assessed thermal stability of submicron microstructures produced by ARB [31.4, 31.5]. Samples with a 250 nm grain size and 0.70 high angle grain boundary (HAGB) fraction were produced with 5 ARB cycles. Short 15-minute static annealing heat treatments were conducted between 200 and 300 °C to simulate necessary preheating time in a load-frame furnace prior to tensile testing at elevated temperatures. Continuous recrystallization, characterized by a reduction in dislocation density, sharpening of deformation texture components and a transition from an elongated to a near-equiaxed grain structure, started to occur at 225 °C [31.4]. This microstructural transition was concurrent with normal grain growth and a loss of submicron ARBed grain structure for annealing times greater than 60 minutes at 250 °C [31.4]. These results suggest limits for low temperature superplasticity: temperatures should be above 225 °C to provide sufficient mobility to accommodate grain boundary sliding, but below 250 °C to avoid deleterious grain growth. These limits will be investigated and formalized through further tensile testing and microstructural analysis.

31.3 Recent Progress

31.3.1 Tensile Testing to Identify Optimal Superplastic Conditions

Tensile tests were conducted for temperatures between 200 and 275 °C and strain rates between 0.0002 and 0.005 s^{-1} to identify parameters that optimize superplasticity. Previous reports [31.4] investigated the effects of static annealing on superplastic performance and concluded that prolonged static annealing led to lower tensile elongations, likely due to a lower dislocation density available to accommodate grain boundary sliding. Overall, extended static annealing was found to be detrimental to superplasticity due to grain growth [31.4]; the as-ARBed condition provided greatest tensile elongations.

Total tensile elongations for the ARBed condition subject to different temperatures and strain rates are summarized in **Figure 31.1a**. While total tensile elongations increase with decreasing strain rate, temperature has a more complicated dependency. Superplasticity is reduced for high (T > 250°C) and low temperatures (T < 225 °C) likely due to grain growth and decreased atomic mobility to accommodate grain boundary sliding, respectively. Moreover, the extent of strain uniformity during deformation can be determined by comparing total tensile elongations in **Figure 31.1a** with the quasi-uniform tensile elongations in **Figure 31.1b**. It can be seen that strain localization in the final neck(s) prior to failure is responsible for roughly 50 to 100 % of total elongation depending on the testing conditions used. Understanding the contribution of final strain localization to overall ductility is pertinent to sheet forming operations, as this thickness variation that occurs during forming may not satisfy dimensional requirements.

Although lower strain rates correlate with higher tensile elongations, **Figure 31.2** shows that strain rate sensitivity (m) values decrease below 0.0005 s^{-1}. This response is typically classified as *regime I creep* as opposed to the *regime II creep* associated with grain boundary sliding and superplastic elongations. There is not a consensus for the root cause of regime I creep in literature. Some authors have reported low strain rate sensitivities due to insufficient stresses to activate multiple slip systems [31.6] while others have suggested a threshold stress for deformation [31.7] or local facets in the grain boundary morphology to be responsible [31.8]. To further complicate matters, the transition to regime I is often reported at strain rates far below what is observed here [31.6–31.8]. Although low strain rate superplasticity is the primary focus for this project, understanding the limits of grain boundary sliding is of significant interest and will be investigated in more detail.

31.3.2 Further Investigation of Optimal Conditions

Enhanced superplasticity through grain refinement can take the form of a superplastic response at reduced temperatures or increased strain rates. Although the primary goal of this project is to investigate low temperature superplasticity, it is also of interest to determine the highest strain rates possible for these reduced temperatures. A higher-temperature, higher-strain-rate condition (250 °C, 0.001 s^{-1}) and a lower-temperature, lower-strain-rate condition (225 °C, 0.0005 s^{-1}) were chosen for a rigorous analysis of the effects of testing parameters on superplastic performance. Both of these conditions accurately fit the reported phenomenological equation for steady-state creep due to grain boundary sliding [31.9]:

$$\dot{\varepsilon} = \frac{DGb}{kT}\left(\frac{d}{b}\right)^{p}\left(\frac{\sigma}{G}\right)^{1/m} \quad [31.1]$$

where D is the diffusivity for grain boundary diffusion, p is the grain size exponent equal to 2 and m is the strain rate sensitivity equal to approximately 0.5. Inverse pole figure (IPF) maps shown in **Figure 31.3** demonstrate the microstructural changes that occur with deformation. Both microstructures first undergo an initial transition from partially elongated grains to near-equiaxed grains until roughly 0.25 true strain. Deformation proceeds with stable grain morphology and texture weakening, both of which are indicative of grain boundary sliding. It is worth noting grain growth is observed in the 250 °C condition, but not in the 225 °C condition.

Representative stress-strain curves for the two conditions are shown in **Figure 31.4** along with the strain rate sensitivity (m) and work hardening coefficient (γ) overlayed as a function of strain. The 225 °C condition shows a slight increase in m values from 0.4 to 0.5 up to 0.5 true strain (e = 0.65). This is consistent with the IPF maps in **Figure 31.4** which show a gradual transition to a more equiaxed grain structure over a similar period of strain. Deformation then proceeds with an m value close to 0.5 until the point of tensile instability at 0.8 true strain (e = 1.22). The 250 °C condition appears to have a microstructure more conducive for grain boundary sliding given that the strain rate sensitivity values stay high and stable until about 0.8 true strain (e = 1.25), at which point final strain localization occurs. Strain rate sensitivities were not determined after the point of final macroscopic necking as the localized strain rate in the neck far exceeds the imposed strain rate.

Dimensional measurements of the cross-section were taken along the gauge length of samples during interrupted testing to determine the extent of strain localization, shown in **Figure 31.5**. In agreement with the work hardening coefficients shown in **Figure 31.4**, both conditions undergo relatively uniform elongation until about 0.75 true strain (e = 1.12). In the 225 °C condition the majority of strain is accommodated in the final neck, whereas the 250 °C demonstrates a more uniform strain distribution.

31.3.3 Biaxal Bulge Testing

Bulge testing was conducted to evaluate superplastic performance with a biaxial strain state. Bulge testing is unique in that it avoids frictional effects associated with hard tooling by using a pressurized fluid, generally hydraulic oil or compressed gas, to deform thin sheets into an open cavity. These experiments are conducted similar to a creep test in that a constant pressure is applied and the sample deforms at steady creep rate. A constant gas pressure was calculated based on uniaxial tensile parameters according to:

$$P = \frac{4\sigma}{S_0 a} e^{\dot{\varepsilon}t} \sqrt{e^{\dot{\varepsilon}t}(1 - e^{\dot{\varepsilon}t})} \qquad [31.2]$$

where P is the pressure necessary to deform a sheet of s_0 thickness and σ stress at $\dot{\varepsilon}$ strain rate over a die cavity of radius a [31.10]. Samples in the ARBed and coarse-grained conditions after interrupted bulge testing are shown in **Figure 31.6** with surface strains measured at the apex of the bulge. The ARBed specimens deformed as predicted and achieved true surface strains of 0.64 and 0.99 for the 225 and 250 °C samples, respectively, after 30 minutes of deformation. Failure proceeded soon after the 30 minute mark at the apex of the bulge. The coarse-grained samples were not able to achieve the anticipated strain rate due to significant work hardening; the 10 μm grain size of these samples is likely more conducive to dislocation creep rather than grain boundary sliding for the conditions tested. The results from these two different microstructures serves as a clear demonstration of the potential capabilities for low temperature superplasticity. Three-dimensional reconstructions of the deformed samples were made using a Keyence imaging system with a variable depth of focus. Height profiles of cross-sections, shown in **Figure 31.7**, will be used along with discretized thickness strains to further characterize formability characteristics.

Plans for Next Reporting Period

For the next reporting period, the following items will be pursued:

- Investigate cavitation damage in interrupted strain (ε = 0.25, 0.50, 0.75, 0.90, 1.00) samples and correlate with onset of tensile instability
- Formalize strain rate and temperature limits for low temperature superplasticity of ARBed material based on kinetics of deformation mechanisms
- Characterize bulge test specimens in terms of strain distribution and cavitation damage

31.4 References

[31.1] Y. Saito, H. Utsunomiya, N. Tsuji, T. Sakai, Novel ultra-high straining process for bulk materials - Development of the accumulative roll bonding (ARB) process, Acta Materialia. 47 (1999) 579–583.

[31.2] S.H. Lee, Y. Saito, N. Tsuji, H. Utsunomiya, T. Sakai, Role of shear strain in ultragrain refinement by accumulative roll-bonding (ARB) process, Scripta Materialia. 46 (2002) 281–285.

[31.3] N. Tsuji, K. Shiotsuki, Y. Saito, Superplasticity of ultra-fine grained Al-Mg alloy by accumulative roll bonding, Mater. Trans. 40 (1999) 765–771.

[31.4] B.N.L. McBride, K.D. Clarke, and A.J. Clarke, Accumulative roll bonding of aluminum sheets toward low temperature superplasticity, CANFSA Report, Project 31, April 2021.

[31.5] B.N.L. McBride, K.D. Clarke, and A.J. Clarke, Mitigation of edge cracking during accumulative roll bonding (ARB) of aluminum strips, Journal of Manufacturing Processes, vol. 55, pp. 236–239, 2020.

[31.6] O. Kaibyshev, Mechanisms of superplastic flow of metals and alloys, Czechoslovak Journal of Physics B. 31 (1981) 223-227.

[31.7] B. Burton, A “creep yield stress” for superplastic deformation, Scripta Materialia. 5 (1971) 669-672.

[31.8] R. Gifkins, Grain boundary sliding and its accommodation during creep and superplasticity, Metallurgical and Materials Transactions A. 7 (1976) 1225-1232.

[31.9] J. Pilling, N. Ridley, Superplasticity in crystalline solids, The Institute of Materials, London, 1984.

[31.10] A. Dutta, A. Mukherjee, Superplastic forming: an analytical approach, Materials Science and Engeering, A. 157 (1992) 9-13.

31.5 Figures and Tables

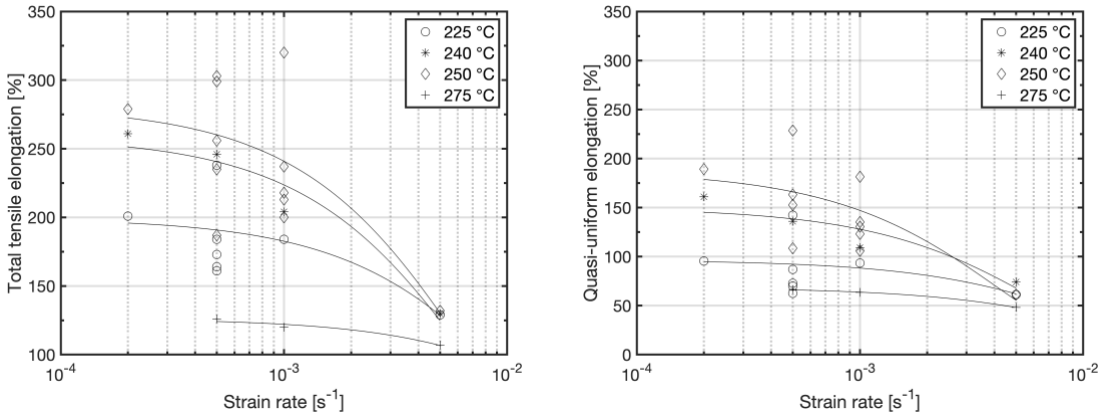

(a) Total tensile elongation (b) Quasi-uniform tensile elongation

Figure 31.1. Total tensile elongations (a) and quasi-uniform tensile elongations (b) for different temperature and strain rate combinations of ARBed material without static annealing. Strain in the final neck is responsible for roughly 100 % strain of the total elongation for strain rates below 0.001 s^{-1}. Anomalously large tensile elongations reported for some conditions are due to the presence of multiple final necks prior to failure.

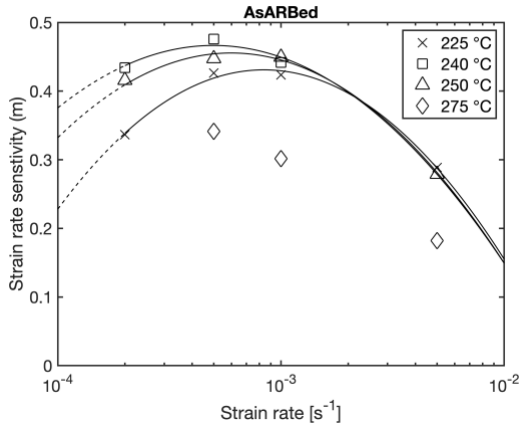

Figure 31.2. Strain rate sensitivities calculated at 0.15 true strain for the ARBed condition plotted as a function of strain rate and temperature. Strain rate sensitivities are highest (m ≈ 0.45) for samples tested between 240 and 250 °C at strain rates between 0.0005 and 0.001 s^{-1} and then continue to decrease for lower strain rates.

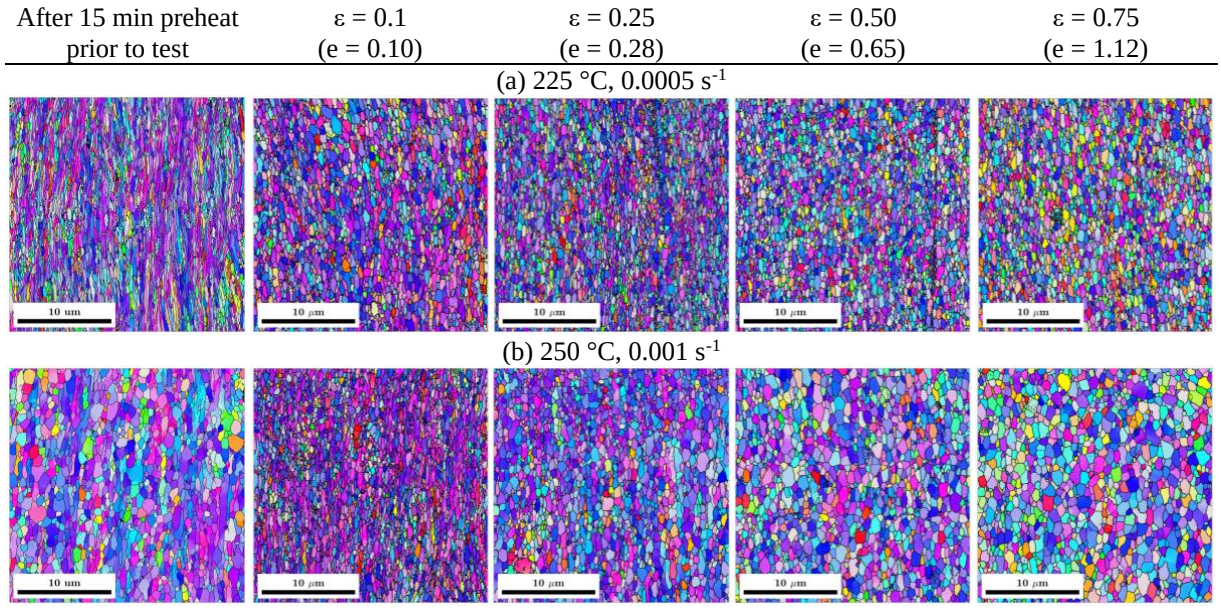

Figure 31.3. Inverse pole figure (IPF) maps showing relative grain size and texture as a function of strain for the (a) 225 °C, 0.0005 s^{-1} and (b) 250 °C, 0.001 s^{-1} conditions. Grains remain near-equiaxed through deformation after an initial transient period up to 0.25 true strain. General texture weaking is observed consistent with grain boundary sliding. All orientations are shown with respect to the normal direction.

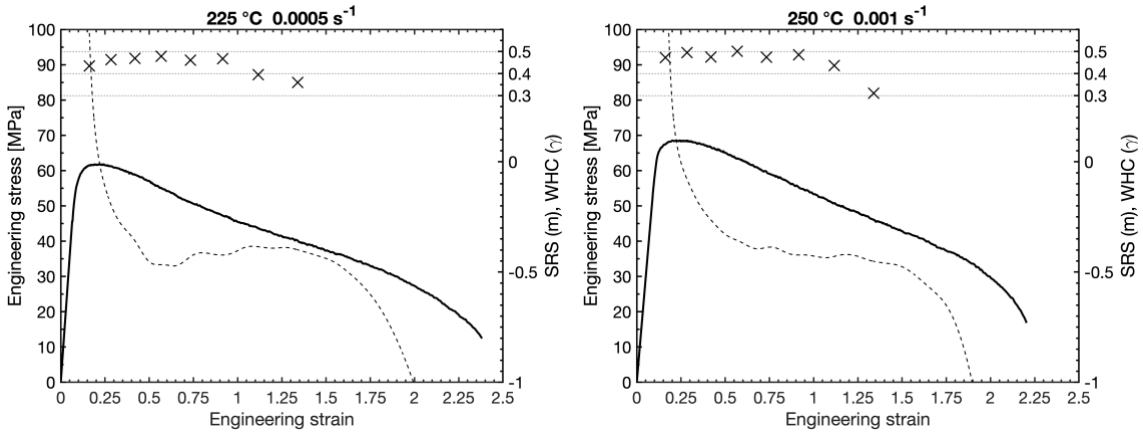

Figure 31.4. Engineering stress strain curves for the (a) 225 °C, 0.0005 s^{-1} condition and (b) 250 °C, 0.001 s^{-1} condition along with the strain rate sensitivity (SRS), *m*, and dimensionless instantaneous work hardening coefficient (WHC), γ.

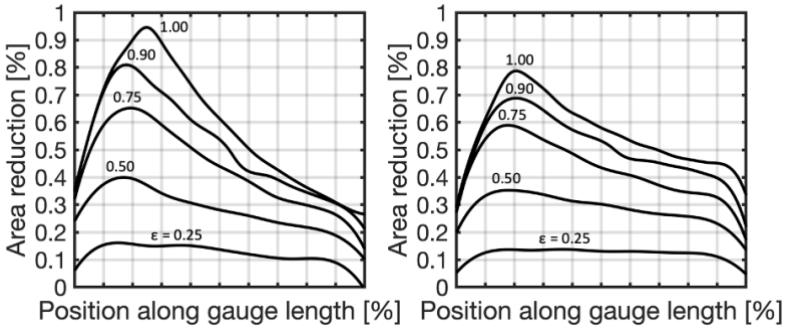

(a) 225 °C, 0.0005 s^{-1} (b) 250 °C, 0.001 s^{-1}

Figure 31.5. Cross-sectional area reduction along the gauge length for interrupted strain tests at true strains ranging from 0.25 to 1.00. The left graph is for a sample tested at 225 °C, 0.0005 s^{-1} while the right graph is for a sample tested at 250 °C, 0.001 s^{-1}. Small variations in area reduction show that strain can localize in regions prior to catastrophic failure. Despite similar total tensile elongations between 200 and 250 %, the sample tested at 250 °C, 0.001 s^{-1} had significantly more uniform elongation along the gauge length.

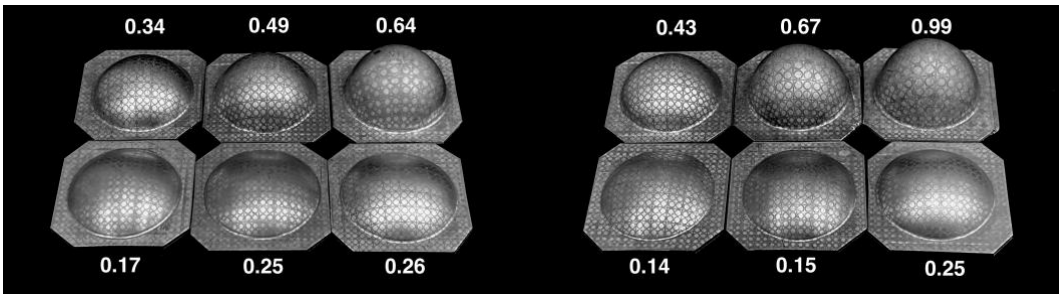

(a) 225 °C (b) 250 °C

Figure 31.6. Biaxial bulge height formability tests conducted at 225 °C (left) and 250 °C (right). Constant pressure Ar gas was used to impose specific strain rates (0.0005 s^{-1} at 225 °C or 0.001 s^{-1} at 250 °C) at the apex of the dome assuming a biaxial hoop stress for 10, 20 or 30 minutes. Samples in the foreground are coarse grained (10 μm) AA 5083; samples in the background are ARBed AA 5083 (~1 μm). The coarse-grained samples did not deform at the intended strain rate due to the inability to achieve grain boundary sliding. The square blanks used for samples were roughly 32 x 32 mm wide and 1 mm thick.

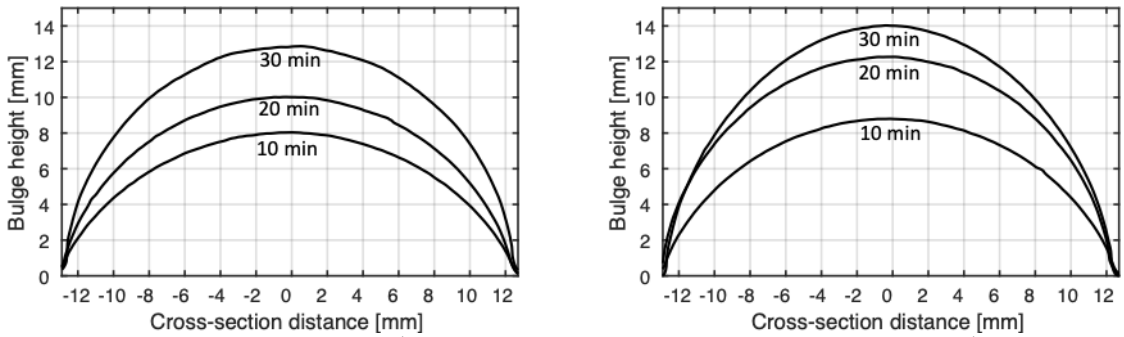

(a) 225 °C, 0.0005 s^{-1} (b) 250 °C, 0.001 s^{-1}

Figure 31.7. Reconstructed bulge height profiles obtained from light optical Keyence imaging for ARBed samples in the 225 °C, 0.0005 s^{-1} condition (left) and the 250 °C, 0.001 s^{-1} condition (right). These profiles will be compared to analytical models to determine formability characteristics.